AGU PUBLICATIONS

Geophysical Research Letters

RESEARCH LETTER
10.1002/2016GL067925

Key Points:
- AMO SSTs are positively correlated with heat fluxes in observations and models with ocean circulation
- The relationship is captured in a simple stochastic model and relies on low-frequency forcing of SST
- This signature is key in reproducing the observed impact of the AMO on European summer temperatures

Supporting Information:
- Supporting Information S1

Correspondence to:
C. H. O'Reilly,
christopher.oreilly@physics.ox.ac.uk

Citation:
O'Reilly, C. H., M. Huber, T. Woollings, and L. Zanna (2016), The signature of low-frequency oceanic forcing in the Atlantic Multidecadal Oscillation, *Geophys. Res. Lett.*, *43*, 2810–2818, doi:10.1002/2016GL067925.

Received 22 JAN 2016
Accepted 24 FEB 2016
Accepted article online 29 FEB 2016
Published online 19 MAR 2016
Corrected 4 JUL 2016

The copyright line for this article was changed on 4 JUL 2016 after original online publication.

The signature of low-frequency oceanic forcing in the Atlantic Multidecadal Oscillation

Christopher H. O'Reilly[1], Markus Huber[1], Tim Woollings[1], and Laure Zanna[1]

[1] Atmospheric, Oceanic and Planetary Physics, Department of Physics, University of Oxford, Oxford, United Kingdom

Abstract The Atlantic Multidecadal Oscillation (AMO) significantly influences the climate of the surrounding continents and has previously been attributed to variations in the Atlantic Meridional Overturning Circulation. Recently, however, similar multidecadal variability was reported in climate models without ocean circulation variability. We analyze the relationship between turbulent heat fluxes and sea surface temperatures (SSTs) over the midlatitude North Atlantic in observations and coupled climate model simulations, both with and without ocean circulation variability. SST anomalies associated with the AMO are positively correlated with heat fluxes on decadal time scales in both observations and models with varying ocean circulation, whereas in models without ocean circulation variability the anomalies are negatively correlated when heat flux anomalies lead. These relationships are captured in a simple stochastic model and rely crucially on low-frequency forcing of SST. The fully coupled models that better capture this signature more effectively reproduce the observed impact of the AMO on European summertime temperatures.

1. Introduction

The AMO has a demonstrable impact on the weather and climate in the continental regions surrounding the North Atlantic basin [*Enfield et al.*, 2001; *Folland et al.*, 1986; *Sutton and Hodson*, 2005; *Knight et al.*, 2006] and is a crucial component in making skillful decadal climate forecasts [*Keenlyside et al.*, 2008]. The AMO has been shown to be related to heat transport by the Atlantic Meridional Overturning Circulation (AMOC) in model experiments [*Delworth et al.*, 1993; *Knight et al.*, 2005; *Latif et al.*, 2004; *Delworth and Mann*, 2000; *Gastineau and Frankignoul*, 2012; *Ba et al.*, 2014], such that the North Atlantic warms when the AMOC speeds up and cools when the AMOC slows down, well reproducing observed multicentury proxy-based sea surface temperature (SST) variability [*Delworth and Mann*, 2000]. However, the observational record of AMOC is too short to directly link its variability to the AMO and alternative mechanisms have been identified as potential drivers of the AMO, questioning the role of AMOC. Recently, a mechanism invoking variability in the wind-driven ocean circulation in the region between the subtropical and subpolar gyres was shown to display good agreement with observations of SST and ocean heat content variability [*McCarthy et al.*, 2015]. Alternatively, some studies have suggested that the variability of aerosol forcing on surface shortwave radiation could have generated the historical AMO variability [*Mann and Emanuel*, 2006; *Booth et al.*, 2012]; however, this has been disputed [*Zhang et al.*, 2013].

Recently, another alternative mechanism for driving the observed AMO variability has been proposed. *Clement et al.* [2015] compared the AMO characteristics in Coupled Model Intercomparison Project Phase 3 (CMIP3) preindustrial control simulations run with a 50 m slab mixed layer ocean model (hereafter "slab ocean" models), which do not permit variability in ocean heat transport, to the AMO characteristics in models coupled to an ocean general circulation model (hereafter "fully coupled" models) and observational SST data sets. The observed "horseshoe" pattern of SST variability associated with the AMO index—defined as the annually averaged, detrended SST anomaly over the North Atlantic basin—is remarkably similar in both slab ocean and fully coupled models (Figure 1). The weaker, tropical part of the AMO SST pattern has been linked to the wind-evaporation-SST feedback [*Xie and Carton*, 2004], which can be captured in slab ocean models. More recently, positive low cloud and dust feedbacks have been implicated for the tropical arm of the AMO [*Yuan et al.*, 2016]. These mechanisms, however, are not effective in the extratropics, where the maximum amplitude of the SST pattern occurs. Since the AMO in the fully coupled and slab ocean models is seemingly indistinguishable, Clement et al. conclude that the AMO SST in midlatitudes must therefore be driven by large-scale atmospheric variability, which is essentially a white noise stochastic process on interannual time

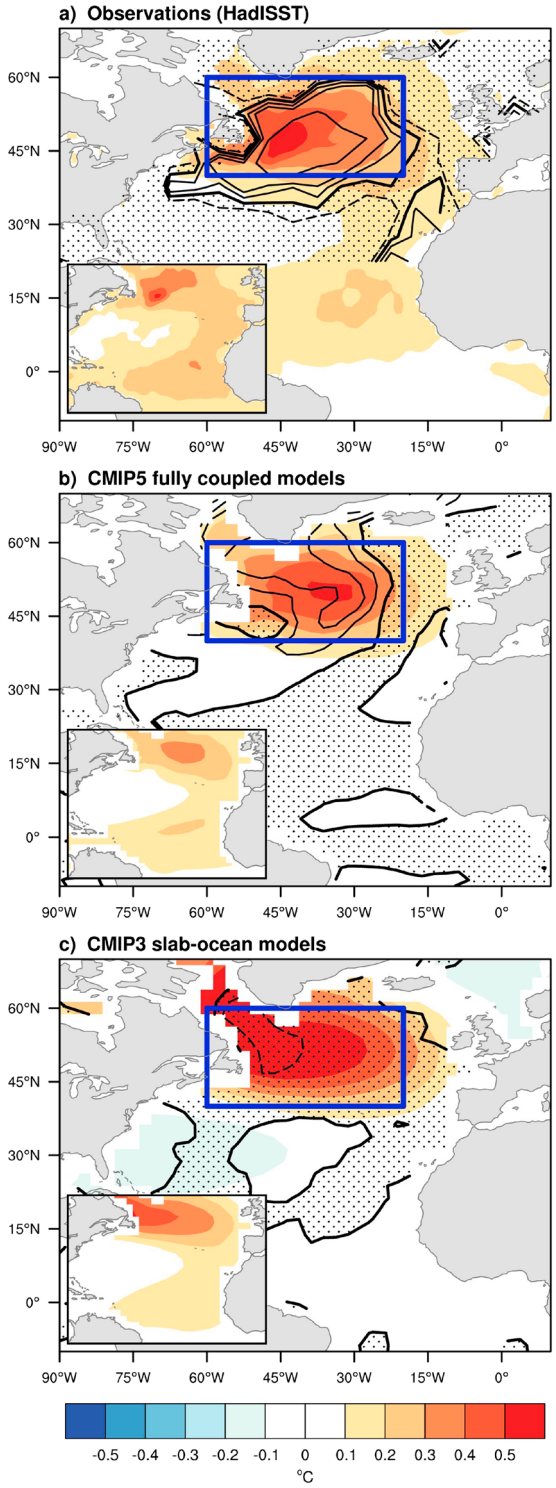

Figure 1. Annual SST anomalies (July through June) regressed onto AMO_{mid}, calculated over the midlatitude North Atlantic (region outlined in blue), and the turbulent heat flux (THF) anomaly averaged over the 10 years prior to the year of the midlatitude AMO indices, in (a) observations (1880–2007); (b) ensemble mean of the CMIP5 preindustrial control simulations; (c) ensemble mean of the CMIP3 slab ocean control simulations. SST anomalies for AMO indices calculated over the whole North Atlantic (80°–0°W, 0°–60°N) are shown in the bottom left of each panel. THF anomalies are contoured at −0.5, 0, 0.5, 1 and 2 W m^{-2}, with negative contours dashed and the zero contour emboldened. Regions of negative THF are stippled. The THF averaged over the region outlined in blue is significantly positive (at the 90% level) in Figure 1a, is positive in more than 90% of the models in Figure 1b, and is negative in more than 90% of the models in Figure 1c.

scales [*Woollings et al.*, 2014]. Here we investigate the source of the AMO, particularly in midlatitudes, in observations, fully coupled CMIP5, and slab ocean CMIP3 control simulations.

2. Data and Methods

2.1. Gridded Observational Data Set

We use the sea surface temperatures (SSTs) from the Hadley Centre sea ice and sea surface temperature data set [*Rayner et al.*, 2003] data set (from 1880 to 2014), the turbulent heat flux (THF) data set (provided over the region 20°–70°N in the North Atlantic) produced by *Gulev et al.* [2013] from the International Comprehensive Ocean-Atmosphere Data Set [*Woodruff et al.*, 2011] (from 1880 to 2007), and the surface air temperatures over land from the Climate Research Unit Time Series [*Harris et al.*, 2014] v. 3.23 (from 1901 to 2014). Annual anomalies are calculated by averaging from July to June.

2.2. Coupled Model Data

We analyze data from the final 127 years of the first member of each of the preindustrial control simulations (*piControl*) in the CMIP5 archive [*Taylor et al.*, 2012], referred to as the fully coupled simulations (only analyzing 41 models that provided THF data). We also analyze data from the CMIP3 models [*Meehl et al.*, 2007] coupled to a slab mixed layer ocean model with a prescribed ocean heat transport, referred to as the slab ocean models. We restrict our analysis of the slab ocean models to only the three models that provided at least 100 years of output, to give a relevant comparison to the observations and CMIP5 fully coupled models. Monthly mean values interpolated the model output on a 2.5×2.5° grid and removed the annual cycle from each model output before calculating the July to June averaged annual anomalies. The results presented here are essentially unchanged if January to December averaged annual anomalies are used instead.

2.3. Monte Carlo Significance Tests

For the regression and correlation calculations, 1000 surrogate indices were produced by taking the fourier transform of the original index and randomizing the phase, thus replicating the spectral properties of the original time series [*Kaplan and Glass*, 2012]. The equivalent regression and correlation statistics were then produced for each of the surrogate indices to give a measure of the significance of the observed relationship. For the difference plot in Figure 2, the 41 models were randomly stratified into 20 warm/cool models 1000 times to give a measure of the chance that the observed correlation difference could occur at random.

3. Relationship Between Turbulent Heat Flux and SST

In the absence of ocean circulation variability (i.e., Ekman currents, heat flux convergence, and entrainment), midlatitude SST anomalies are directly forced by turbulent (i.e., latent plus sensible) heat fluxes [*Deser et al.*, 2010] (THFs). To focus on the midlatitude maximum in the AMO SST pattern, we define a midlatitude AMO index, AMO_{mid}, over the region which exhibits the largest multidecadal variability in observations [*Gulev et al.*, 2013]. AMO_{mid} is defined as the area average of annual mean detrended SST anomalies over the region (60°–20°W, 40°--60°N). The results presented here are not sensitive to adjustments in the region used to define AMO_{mid} within the midlatitudes but the results degrade when SST anomalies south of about 35°N are included, which is consistent with other mechanisms being important in generating the tropical part of the AMO pattern. AMO_{mid} well captures the full AMO SST pattern in the northern part of the basin and even much of the tropical SST pattern in the observations (Figure 1). The AMO_{mid} index and the AMO averaged over the whole North Atlantic are very closely correlated, with a correlation coefficient of 0.97.

To see the role of THFs in driving the AMO on decadal time scales, the THF anomalies (defined as positive upwards) were averaged over the preceding 10 years and regressed onto AMO_{mid} (Figure 1). In observations, it has been shown that on decadal time scales the THF and SST anomalies are positively correlated in the midlatitude North Atlantic [*Gulev et al.*, 2013] and here we see that the midlatitude THF is positive over the decade preceding a warm SST anomaly. In the fully coupled models the THF over the preceding decade is also positive, albeit weaker than in the observations. In the slab ocean models, however, a decade of negative midlatitude THF leads to a year with a warm SST anomaly, unlike in the observations or fully coupled models. The negative midlatitude THFs in the slab ocean models heat the ocean mixed layer and result in a warm AMO_{mid}. In contrast, positive midlatitude THFs in the observations and fully coupled models cool the ocean mixed layer. Therefore, an additional mechanism that is most likely related to ocean circulation variability, which is not present in the slab ocean models, must be providing additional heating to the mixed layer in the midlatitude North Atlantic.

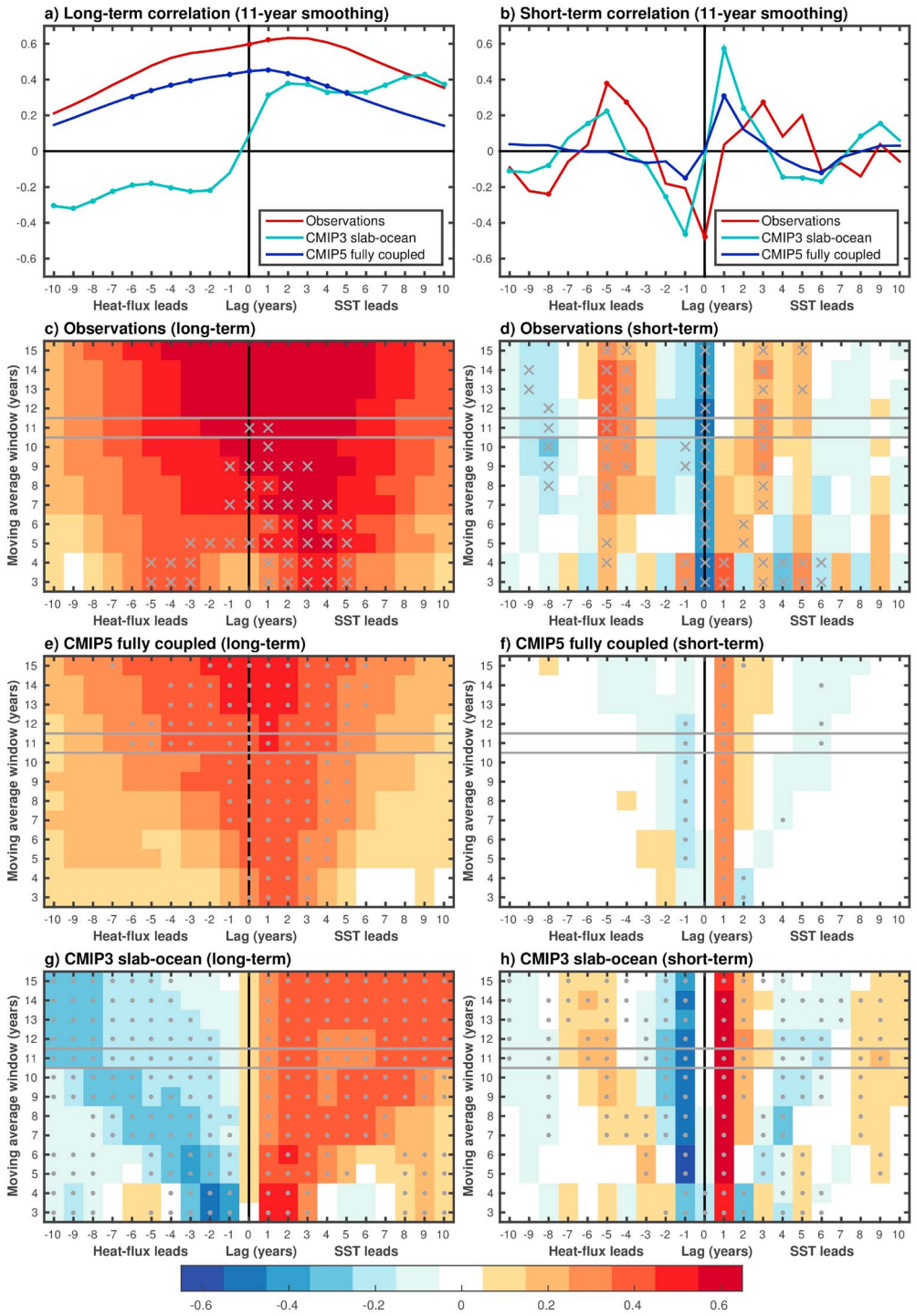

Figure 2. Impact of low-frequency forcing of the AMO_{mid} on summertime European temperatures. (a) Observations of the summertime (June–August) surface air temperature (SAT) over land and SST anomalies over ocean, regressed onto the 11 year moving average of AMO_{mid}. (b) Model mean of the SAT anomalies regressed onto the 11 year moving average of AMO_{mid}, in the 20 models with the warmest SAT anomaly regression averaged over the North Atlantic/European region (outlined in black). (c) As in Figure 2b but for the 20 models with the coolest SAT anomaly regression. (d and e) The correlation between the long-term components of the THF and SST for the 20 warm and cool models, respectively, and (f) the difference in correlation (i.e., warm models minus cold models). The stippling in Figure 2a indicates where the SAT regression is significant at the 90% level. The grey crosses in Figure 2f indicate where the difference between the correlations in the warm and cool are significant at the 90% level (calculated using a Monte Carlo resampling).

To further characterize the relationship between THFs and midlatitude SST anomalies, we now analyze lead-lag correlations at different time scales. We decompose AMO_{mid} into $AMO_{mid} = \overline{AMO_{mid}} + AMO'_{mid}$, where the long-term component ($\overline{AMO_{mid}}$) is calculated using a moving average (of varying length) and the short-term component (AMO'_{mid}) is the residual of $\overline{AMO_{mid}}$; an equivalent separation is also performed on the THF (i.e., $Q = \overline{Q} + Q'$). It has previously been shown in observations that the long-term components of THF and midlatitude SST anomalies are positively correlated at zero lag [*Gulev et al.*, 2013]. Interestingly, the observed long-term THF and SST anomalies are also positively correlated when either the THF or SST leads by up to a decade (Figures 3a and 3c). The short-term components, however, are negatively correlated at zero lag (Figures 3b and 3d), reflecting the relatively passive response of the midlatitude ocean to atmospheric forcing on interannual time scales [*Gulev et al.*, 2013; *Deser et al.*, 2010].

The ensemble mean of the correlation between the long-term THF and SST components in the fully coupled models is also positively correlated at zero lag (Figures 3a and 3e). The correlations are generally smaller than in the observations at all lags and time scales, but a significant majority of the fully coupled models capture the overall structure, showing strongly positive correlations when either the THF or SST leads by up to a decade. In the slab ocean models, however, the long-term components differ substantially from the observations and fully coupled models, depending critically on lag. When the THF leads, the correlation is negative at nearly all timescales, whereas when the SST leads, the correlation is positive at nearly all time scales. Therefore, when the THF leads in the slab ocean models, an extended period of negative THF warms the mixed layer and results in a warm SST anomaly. This warm SST anomaly is then damped by the atmosphere over time, resulting in positive THFs over the subsequent period. Similar long-term warm SST anomalies in the observations and fully coupled models tend to lag periods of positive THF, which act to cool the mixed layer, therefore something other than THF must be forcing the long-term SST anomalies. Interestingly, the fully coupled or slab ocean models are similarly unable to reproduce the negative correlation between the short-term THF and SST components at zero lag seen in the observations (Figures 3a, 3f, and 3h). The correlations were calculated using annual averages, indicating that the models may poorly represent the THF and SST variability on intra-annual time scales (similar correlations are seen if January to December averages are used). It is noteworthy that the largest spread in short-term correlations among the fully coupled models occurs at zero lag, suggesting some inconsistency between the models themselves (supporting information Figure S1). The stronger correlation between the short-term components in the slab ocean models, compared with the fully coupled models, may be related to the underestimation of mixed layer depth (50 m) in these models, such that there is greater SST response for the same turbulent heat flux anomaly.

4. Stochastic Model of Midlatitude AMO Variability

To further understand the relationships between THF and SST seen in the models and observations, we consider a simple stochastic climate model. Such models have previously proven very effective in capturing key features of midlatitude SST variability [*Frankignoul and Hasselmann*, 1977; *Deser et al.*, 2003; *Barsugli and Battisti*, 1998; *Bretherton and Battisti*, 2000]. In our stochastic model the SST anomaly (T) follows

$$\frac{dT}{dt} = Q + F_{ocean} = -\lambda T + Q_{atmos} + F_{ocean} \quad (1)$$

where the total THF anomaly (Q) is composed of a damping term (with a constant timescale $\lambda^{-1} = 4$ years, to represent the persistence and/or reemergence of annual midlatitude SST anomalies) and a stochastic atmospheric forcing term ($Q_{atmos} = A_{hf}dW$, where $A_{hf} = 0.1°C\ yr^{-1}$ is a constant amplitude and dW is a Gaussian white noise process with unit variance). A periodic forcing term ($F_{ocean} = A_{lf} \sin\left(\frac{2\pi t}{\tau_{lf}}\right)$, where $A_{lf} = 0.04°C\ yr^{-1}$ is a constant amplitude and $\tau_{lf} = 60$ years is the period) is added to mimic the presence of low-frequency variability in ocean heat transport. These values were chosen to approximately capture the variability of the observed AMO index in this region (see example time series in supporting information Figure 2). The stochastic model is run for 1000 ensemble members, each for 127 years to match the observations. To analyze the signature of ocean circulation variability, the model is also run without the low-frequency forcing term (i.e., $F_{ocean} = 0$). Without the low-frequency forcing term, the variance of the SST in the stochastic model is reduced but this has no influence on the correlation statistics.

In the presence of low-frequency ocean forcing, the ensemble mean correlation between the long-term THF and SST components in the stochastic model is positive when either THF or SST leads by up to a decade (Figures 4a and 4c). This corresponds closely to the relationship between the long-term components of THF

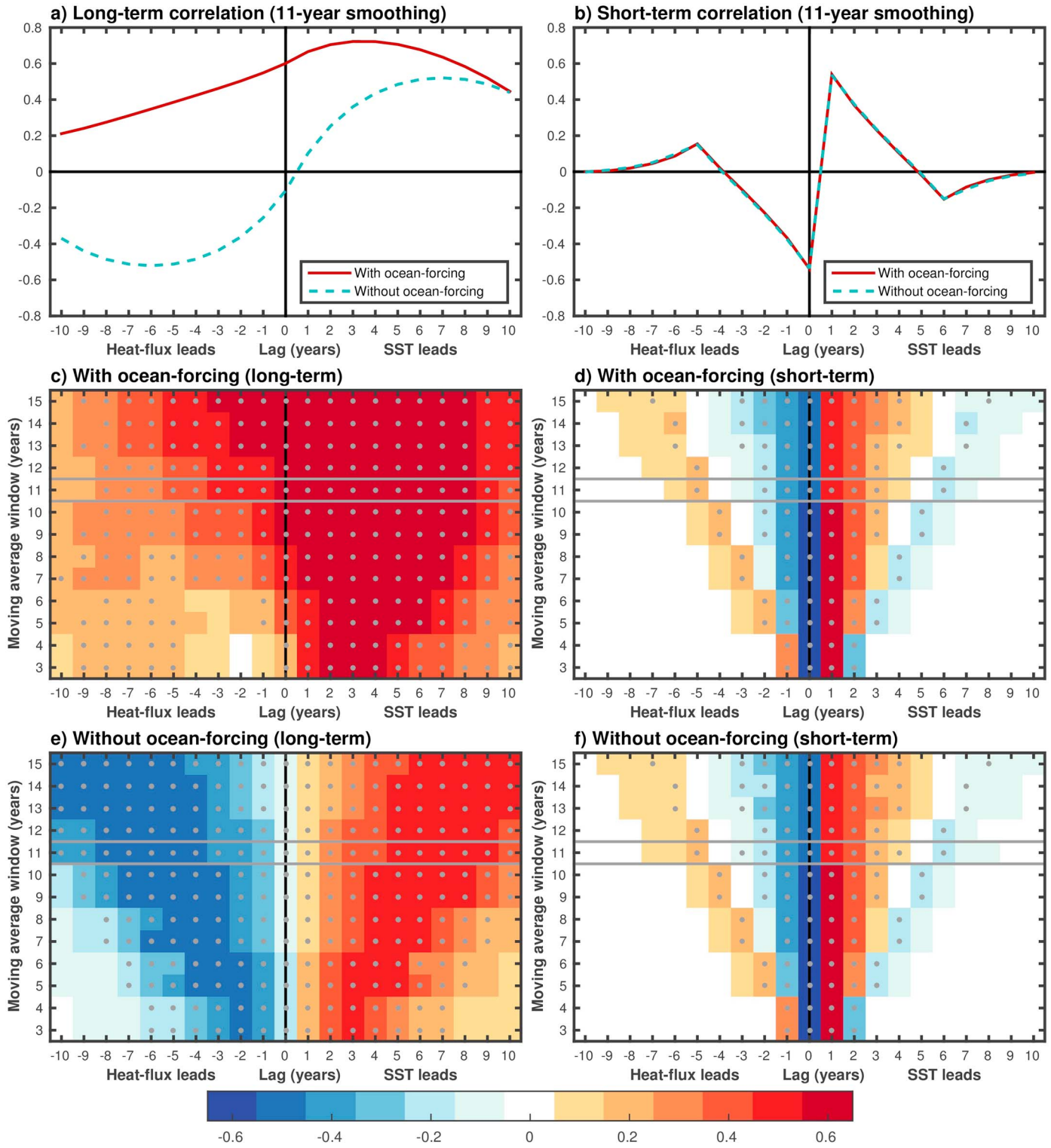

Figure 3. Correlation between AMO_{mid} and THF anomalies (averaged over the same midlatitude North Atlantic region, outlined in Figure 1) for the long-term (left column) and short-term (right column) components: (a and b) Correlations at different lags for an 11 year smoothing window; (c and d) correlations in the observations (1880–2007) for different moving average windows; (e and f) ensemble mean correlations for the CMIP5 preindustrial control simulations for different moving average windows; and (g and h) ensemble mean correlations from the CMIP3 slab ocean control simulations for different moving average windows. The long-term components are calculated using a moving average and the short-term components are the residual. The grey lines in Figures 3c–3h highlight the 11 year moving average window. In Figures 3c and 3d the grey crosses indicate where the correlation is significant at the 90% level. In Figures 3e–3h, the dots indicate where the correlation has the same sign in more than 90% of the models. Correlations that are significant at the 90% level or have the same sign in more than 90% of the models are indicated by circles in Figures 3a and 3b.

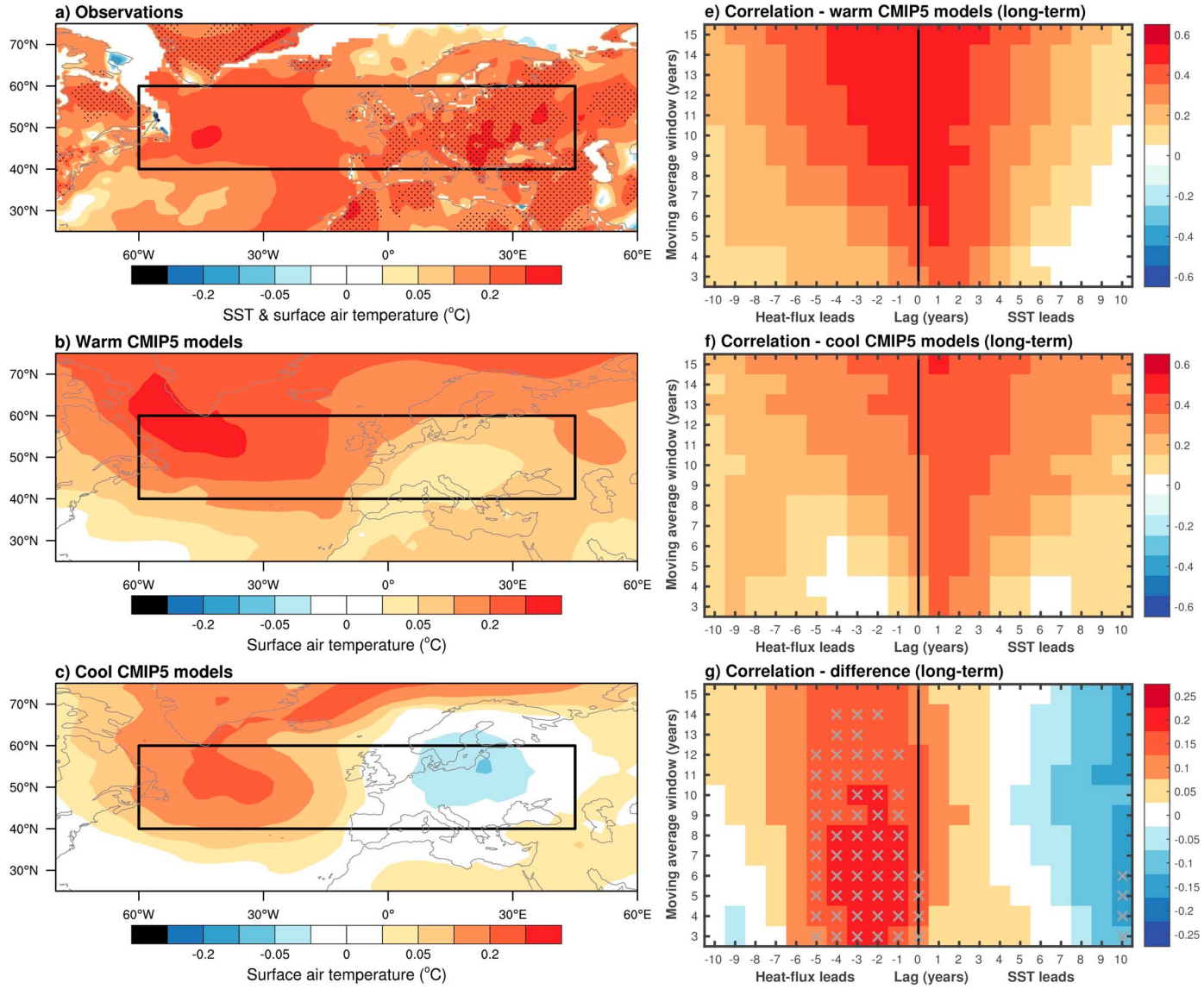

Figure 4. Correlations between the SST and THF anomalies for (left column) long-term and (right column) short-term components in the 1-D stochastic model, averaged over 1000 separate realizations of 127 years, all with parameters $A_{hf} = 0.1°C\ yr^{-1}$, $\lambda^{-1} = 4$ years, and $\tau_{lf} = 60$ years: (a and b) correlations at different lags for an 11 year smoothing window. (c and d) Correlations for different moving average windows with ocean forcing ($A_{lf} = 0.04°C\ yr^{-1}$) and (e and f) without ocean forcing ($A_{lf} = 0$). The grey lines in Figures 4c–4f highlight the 11 year moving average window. Dots indicate where the correlation has the same sign in more than 90% of the individual realizations.

and SST in the observations and fully coupled models (Figures 3a, 3c, and 3e). Without low-frequency ocean forcing, the correlation between the long-term THF and SST components in the stochastic model is negative for all time scales when the THF leads but is positive when the SST leads (Figures 4b and 4d). This closely corresponds to the relationship between the long-term THF and SST components in the slab ocean models (Figures 3a and 3g). The correlation between the short-term components of THF and SST in the stochastic model is negative at zero lag and essentially identical both with and without low-frequency ocean forcing (Figures 4b, 4d, and 4f), in agreement with the observed interannual correlation (Figures 3b and 3d). These results are insensitive to changes in the damping time scale λ^{-1}, providing it is sufficiently shorter than the timescale of the low-frequency forcing term. The simple stochastic model therefore highlights the importance of a low-frequency forcing term in reproducing the relationship between THF and SST seen in the observations and the fully coupled models, whereas the relationship between THF and SST seen in the slab ocean models is well captured by a model only forced with stochastic atmospheric forcing.

5. Importance of Low-Frequency Forcing in Fully Coupled Models

The AMO has an observed influence on the decadal variability of summertime surface air temperatures (SAT) over Europe as well as over the North Atlantic ocean [*Sutton and Dong*, 2012] (Figure 2a). To assess the importance of low-frequency ocean forcing on the decadal variability of surface temperatures the 11 year averaged AMO_{mid} was regressed onto SAT in each of the 41 fully coupled models. We averaged the resulting SAT regression over a midlatitude North Atlantic/Europe region (black box in Figures 2a–2c) and stratified the models into groups of the 20 warmest and coolest SAT. The warmest models have a SAT pattern which is fairly similar to that seen in observations and is warmer than the coolest models over both the North Atlantic and Europe (Figures 2b and 2c). The warmest models exhibit large correlations between the long-term components of THF and SST when THF leads. Conversely, the coolest models exhibit a significantly weaker positive correlation when the THF leads (Figures 2f and 2g), indicating that these models tend to have a weaker low-frequency ocean forcing. In agreement with this, the slab ocean models also fail to capture the warming over Europe during positive AMO_{mid} (supporting information Figure S3). Therefore, the models that best capture the observed response to AMO_{mid} clearly exhibit a stronger signature of low-frequency ocean forcing (i.e., Figure 4). This implies that it is heat released by the ocean that leads to warming over Europe during the warm phase of the AMO.

6. Conclusions

While slab ocean models are able to produce SST patterns and statistics similar to those seen fully coupled models and observations, here we have shown that only fully coupled models are able to correctly reproduce the observed relationship between THF and SST in midlatitudes on decadal time scales. The slab ocean models respond passively to stochastic atmospheric forcing, whereas the fully coupled models and observations both exhibit positive correlations between THF and SST when either leads by up to a decade, which is shown to be a signature of low-frequency ocean forcing in a simple stochastic model. While we cannot make the link directly, by far the most plausible explanation is ocean circulation variability, which is not present in the slab ocean models. The source of the ocean circulation variability in the North Atlantic may be due to wind-driven circulation anomalies [*McCarthy et al.*, 2015] or AMOC variability [*Delworth et al.*, 1993; *Knight et al.*, 2005; *Latif et al.*, 2004; *Delworth and Mann*, 2000; *Ba et al.*, 2014], but it is clear from our analysis that the observed AMO is not directly forced by stochastic atmospheric forcing in midlatitudes. Capturing the signature of low-frequency ocean forcing in fully coupled models is found to be crucially important in correctly representing the influence of AMO_{mid} on summertime European temperatures, indicating that models that better represent low-frequency forcing of SST are more reliable for making decadal predictions.

Acknowledgments
We thank two anonymous reviewers for their insightful comments and useful suggestions. The work by C.O.R., T.W., and L.Z. was supported by the NERC SummerTIME project (grant number NE/M005887/1). M.H. was supported by the Swiss National Science Foundation grant P300P2_158448. We acknowledge the World Climate Research Programme's Working Group on Coupled Modelling, which is responsible for CMIP, and we thank the climate modeling groups for producing and making available their model output. For CMIP the U.S. Department of Energy's Program for Climate Model Diagnosis and Intercomparison provides coordinating support and led development of software infrastructure in partnership with the Global Organization for Earth System Science Portals. We thank ETHZ for access to their CMIP data archive. We acknowledge the authors of *Gulev et al.* [2013] for providing the observational heat flux data used here, which is available online (http://www.nature.com/nature/journal/v499/n7459/extref/nature12268-s2.zip). We also thank Antje Weisheimer for useful comments on an earlier version of the manuscript.

References

Ba, J., et al. (2014), A multi-model comparison of Atlantic multidecadal variability, *Clim. Dyn.*, *43*(9–10), 2333–2348.
Barsugli, J. J., and D. S. Battisti (1998), The basic effects of atmosphere-ocean thermal coupling on midlatitude variability*, *J. Atmos. Sci.*, *55*(4), 477–493.
Booth, B. B., N. J. Dunstone, P. R. Halloran, T. Andrews, and N. Bellouin (2012), Aerosols implicated as a prime driver of twentieth-century North Atlantic climate variability, *Nature*, *484*(7393), 228–232.
Bretherton, C. S., and D. S. Battisti (2000), An interpretation of the results from atmospheric general circulation models forced by the time history of the observed sea surface temperature distribution, *Geophys. Res. Lett.*, *27*(6), 767–770.
Clement, A., K. Bellomo, L. N. Murphy, M. A. Cane, T. Mauritsen, G. Rädel, and B. Stevens (2015), The Atlantic Multidecadal Oscillation without a role for ocean circulation, *Science*, *350*(6258), 320–324.
Delworth, T., S. Manabe, and R. Stouffer (1993), Interdecadal variations of the thermohaline circulation in a coupled ocean-atmosphere model, *J. Clim.*, *6*(11), 1993–2011.
Delworth, T. L., and M. E. Mann (2000), Observed and simulated multidecadal variability in the Northern Hemisphere, *Clim. Dyn.*, *16*(9), 661–676.
Deser, C., M. A. Alexander, and M. S. Timlin (2003), Understanding the persistence of sea surface temperature anomalies in midlatitudes, *J. Clim.*, *16*(1), 57–72.
Deser, C., M. A. Alexander, S.-P. Xie, and A. S. Phillips (2010), Sea surface temperature variability: Patterns and mechanisms, *Mar. Sci.*, *2*, 115–143.
Enfield, D. B., A. M. Mestas-Nunez, and P. J. Trimble (2001), The Atlantic multidecadal oscillation and its relation to rainfall and river flows in the continental U.S., *Geophys. Res. Lett.*, *28*(10), 2077–2080.
Folland, C., T. Palmer, and D. Parker (1986), Sahel rainfall and worldwide sea temperatures, 1901–85, *Nature*, *320*(6063), 602–607.
Frankignoul, C., and K. Hasselmann (1977), Stochastic climate models. Part II. application to sea-surface temperature anomalies and thermocline variability, *Tellus*, *29*(4), 289–305.
Gastineau, G., and C. Frankignoul (2012), Cold-season atmospheric response to the natural variability of the Atlantic meridional overturning circulation, *Clim. Dyn.*, *39*(1–2), 37–57.
Gulev, S. K., M. Latif, N. Keenlyside, W. Park, and K. P. Koltermann (2013), North Atlantic Ocean control on surface heat flux on multidecadal timescales, *Nature*, *499*(7459), 464–467.

Harris, I., P. Jones, T. Osborn, and D. Lister (2014), Updated high-resolution grids of monthly climatic observations – The CRU TS3. 10 Dataset, *Int. J. Climatol.*, *34*(3), 623 – 642.

Kaplan, D., and L. Glass (2012), *Understanding Nonlinear Dynamics*, Springer, New York.

Keenlyside, N., M. Latif, J. Jungclaus, L. Kornblueh, and E. Roeckner (2008), Advancing decadal-scale climate prediction in the North Atlantic sector, *Nature*, *453*(7191), 84 – 88.

Knight, J. R., R. J. Allan, C. K. Folland, M. Vellinga, and M. E. Mann (2005), A signature of persistent natural thermohaline circulation cycles in observed climate, *Geophys. Res. Lett.*, *32*, L20708, doi:10.1029/2005GL024233.

Knight, J. R., C. K. Folland, and A. A. Scaife (2006), Climate impacts of the Atlantic multidecadal oscillation, *Geophys. Res. Lett.*, *33*, L17706, doi:10.1029/2006GL026242.

Latif, M., E. Roeckner, M. Botzet, M. Esch, H. Haak, S. Hagemann, J. Jungclaus, S. Legutke, S. Marsland, and U. Mikolajewicz (2004), Reconstructing, monitoring, and predicting multidecadal-scale changes in the North Atlantic thermohaline circulation with sea surface temperature, *J. Clim.*, *17*(7), 1605 – 1614.

Mann, M. E., and K. A. Emanuel (2006), Atlantic hurricane trends linked to climate change, *Eos Trans. AGU*, *87*(24), 233 – 244.

McCarthy, G. D., I. D. Haigh, J. J.-M. Hirschi, J. P. Grist, and D. A. Smeed (2015), Ocean impact on decadal Atlantic climate variability revealed by sea-level observations, *Nature*, *521*(7553), 508 – 510.

Meehl, G. A., C. Covey, K. E. Taylor, T. Delworth, R. J. Stouffer, M. Latif, B. McAvaney, and J. F. Mitchell (2007), The WCRP CMIP3 multimodel dataset: A new era in climate change research, *Bull. Am. Meteorol. Soc.*, *88*(9), 1383 – 1394.

Rayner, N., D. E. Parker, E. Horton, C. Folland, L. Alexander, D. Rowell, E. Kent, and A. Kaplan (2003), Global analyses of sea surface temperature, sea ice, and night marine air temperature since the late nineteenth century, *J. Geophys. Res.*, *108*(D14), 4407, doi:10.1029/2002JD002670.

Sutton, R. T., and B. Dong (2012), Atlantic Ocean influence on a shift in European climate in the 1990s, *Nat. Geosci.*, *5*(11), 788 – 792.

Sutton, R. T., and D. L. Hodson (2005), Atlantic Ocean forcing of North American and European summer climate, *Science*, *309*(5731), 115 – 118.

Taylor, K. E., R. J. Stouffer, and G. A. Meehl (2012), An overview of CMIP5 and the experiment design, *Bull. Am. Meteorol. Soc.*, *93*(4), 485 – 498.

Woodruff, S. D., et al. (2011), ICOADS release 2.5: Extensions and enhancements to the surface marine meteorological archive, *Int. J. Climatol.*, *31*(7), 951 – 967.

Woollings, T., C. Czuchnicki, and C. Franzke (2014), Twentieth century North Atlantic jet variability, *Q. J. R. Meteorol. Soc.*, *140*(680), 783 – 791.

Xie, S.-P., and J. A. Carton (2004), Tropical Atlantic variability: Patterns, mechanisms, and impacts, in *Earth Climate: The Ocean-Atmosphere Interaction*, vol. 147, edited by C. Wang, S.-P. Xie, and J. A. Carton, pp. 121 – 142, AGU, Washington, D. C.

Yuan, T., L. Oreopoulos, M. Zelinka, H. Yu, J. Norris, M. Chin, S. Platnick, and K. Meyer (2016), Positive low cloud and dust feedbacks amplify tropical North Atlantic multidecadal oscillation, *Geophys. Res. Lett.*, *43*, doi:10.1002/2016GL067679, in press.

Zhang, R., et al. (2013), Have aerosols caused the observed Atlantic multidecadal variability?, *J. Atmos. Sci.*, *70*(4), 1135 – 1144.

Geophysical Research Letters

Supporting Information for

The signature of low frequency forcing in the Atlantic Multidecadal Oscillation

Christopher H. O'Reilly, Markus Huber, Tim Woollings, Laure Zanna

Atmospheric, Oceanic and Planetary Physics, Department of Physics, University of Oxford.

Contents of this file

Figures S1 to S3
Tables S1 to S2

Introduction

This file includes 3 supplementary figures which are closely related to the figures in the main text. Also included is are lists of the coupled model simulations used in our study.

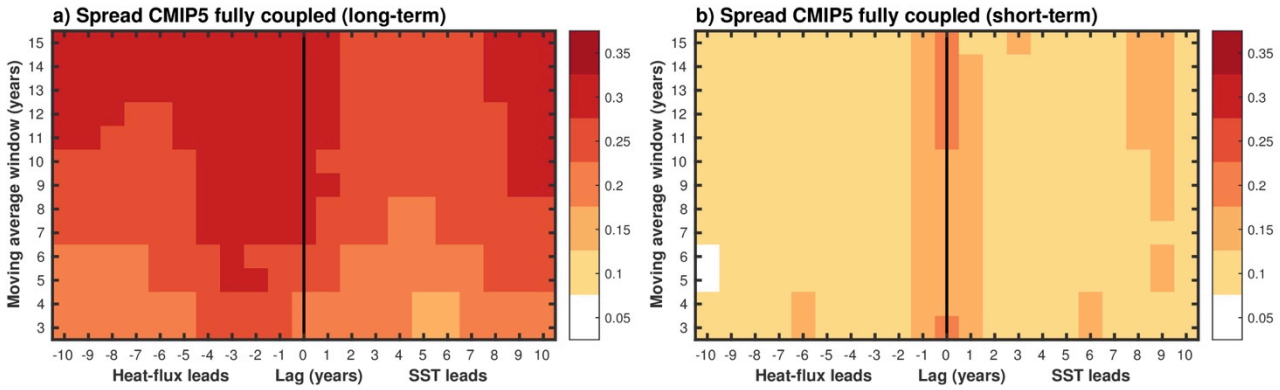

Figure S1. Spread of the correlations of the individual CMIP5 fully coupled models, whose ensemble mean correlations are shown in Figure 2.

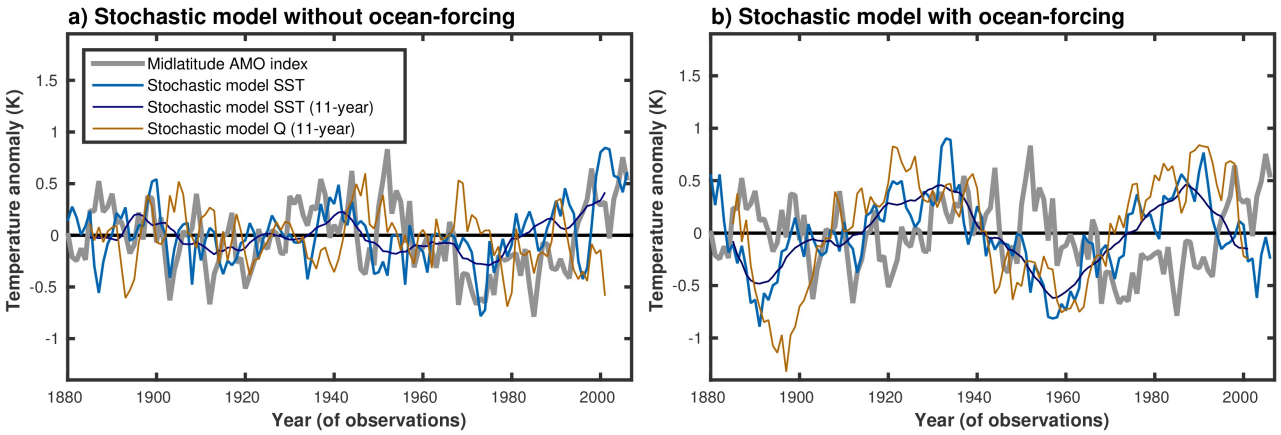

Figure S2. Example time series from a single realization of the stochastic model described in the main text, (a) without and (b) with low frequency ocean forcing. Te observed AMO_{mid} is plotted for comparison.

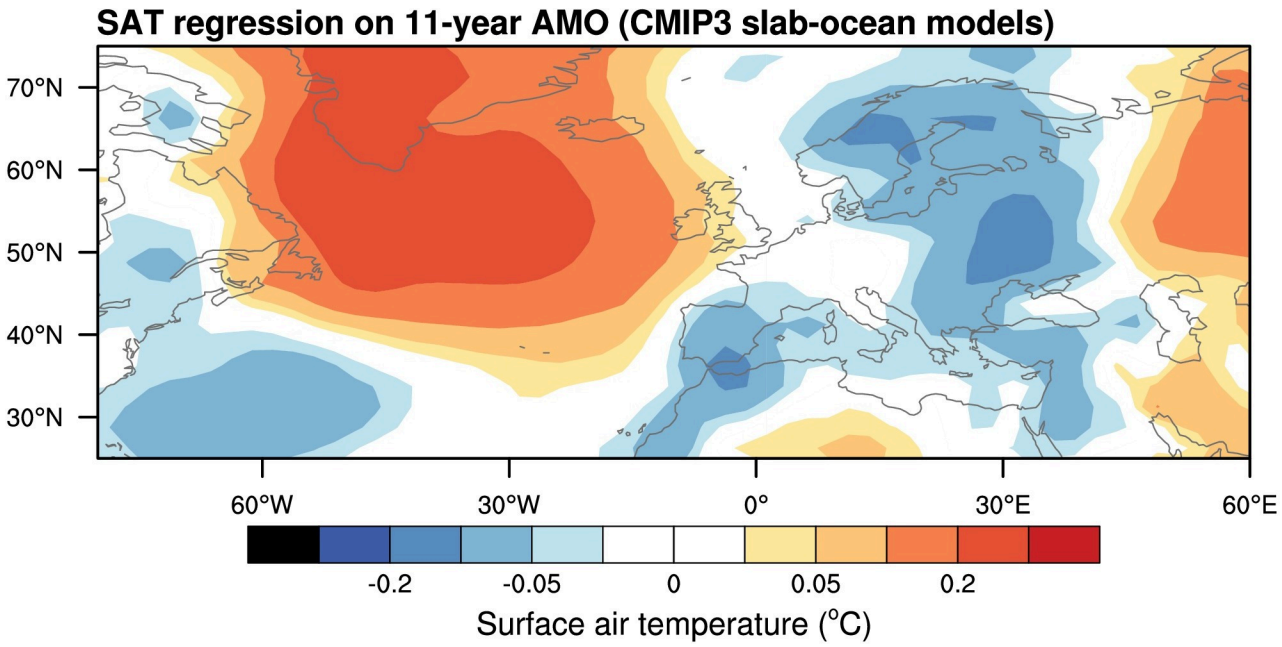

Figure S3. Ensemble mean of the JJA surface air temperature (SAT) regressed on the the normalised 11-year averaged midlatitude AMO index in the CMIP3 slab ocean models. Note the impact is very different over Europe compared to the observations and the "warm" fully coupled models (i.e. Figure 4).

Model name	Length of integration (in years)
GISS_MODEL_E_R	120
MRI_CGCM2_3_2A	100
MPI_ECHAM5	100

Table S1. List of slab-ocean CMIP3 models used in the study. Only models that provided data for at least 100 years were included.

Model name	Warm/Cool AMO over Europe
ACCESS1-0	Warm
ACCESS1-3	Warm
BCC-CSM1-1	Cool
BCC-CSM1-1-M	Cool
BNU-ESM	Warm
CCSM4	Cool
CESM1-BGC	Cool
CESM1-CAM5	Cool
CESM1-CAM5-1-FV2	Cool
CESM1-FASTCHEM	Cool
CESM1-WACCM	Cool
CMCC-CESM	Cool
CMCC-CM	Warm
CMCC-CMS	Warm
CNRM-CM5	Cool
CSIRO-Mk3-6-0	Warm
CanESM2	Cool
FGOALS-s2	Cool
FIO-ESM	Warm
GFDL-CM3	Warm
GFDL-ESM2G	Warm
GFDL-ESM2M	Warm
GISS-E2-H	Cool
GISS-E2-H-CC	Cool
GISS-E2-R	Warm
GISS-E2-R-CC	Cool
HadGEM2-CC	Warm
HadGEM2-ES	Warm
INM-CM4	Warm
IPSL-CM5A-LR	Warm
IPSL-CM5A-MR	Neither
IPSL-CM5B-LR	Warm
MIROC-ESM	Cool
MIROC-ESM-CHEM	Warm
MIROC5	Warm
MPI-ESM-LR	Warm
MPI-ESM-MR	Warm
MPI-ESM-P	Cool
MRI-CGCM3	Cool
NorESM1-M	Cool
NorESM1-ME	Cool

Table S2. A list of the preindustrial control CMIP5 models used in our study. The column on the right indicates which models were classified as having a warm and cool response to the AMO (i.e. Figure 4). See the main text for further details.